V European Conference on Computational Fluid Dynamics
ECCOMAS CFD 2010
J. C. F. Pereira and A. Sequeira (Eds)
Lisbon, Portugal, 14–17 June 2010

A METHOD OF CONSISTENT AVERAGES FOR THE COMPUTATIONAL SOLUTION TO THE FLUID DYNAMICS EQUATIONS

Frederick Ferguson[*], Gafar Elamin[†], and Mookesh Dhanasar[††]

[*]North Carolina A&T State University
1601 East Market Street, Greensboro, NC 27411
e-mail: fferguso@ncat.edu

[††] North Carolina A&T State University
Center for Aerospace Research, 2105 Yanceyville Street, NC 27405
mdhanasar@yahoo.com

Key words: Integral-Differential Scheme (IDS), Method of Consistent Averages (MCA), Navier-Stokes Equations, Finite Volume, Hypersonic, Cavity Driven Flows

Abstract. *The goal of this research effort is to improve the efficiencies of CFD tools by focusing on the development of a robust, efficient, and accurate numerical framework that is capable of solving a variety of complex fluid dynamics problems; overcoming several limitations of well-established schemes. The new scheme, termed the 'Method of Consistent Averages' (MCA)[1], has the following features:*

1. The scheme is developed on the basis of a unique combination of the differential and integral forms of the Navier-Stokes equations. As such, the scheme has the potential to accurately capture the flow physics.

2. This scheme guarantees continuity of the numerical flux quantities rather than manipulating the primitive flowfield variables to ensure continuity.

3. An accurate accounting of the mass, momentums, and energy fluxes is considered at two major locations; the center of the numerical control volume, and at each of the surface making up the volume of interest.

The MCA numerical process is developed herein is based on two fundamental types of control volumes; namely, spatial cells and temporal cells. A typical spatial cell is developed from eight neighbouring node, where as, a typical temporal cell is developed from the center node of eight neighbouring cells. In this analysis, a control volume is composed of a collection of eight spatial cells and one temporal cell, and numerically described by the ijk-point. The final solution at node i,j,k is developed from a system of carefully crafted control volumes. The contributions of these nodes to the final solution at node i,j,k are dictated by the fluid dynamic conservation laws.

1 INTRODUCTION

A historic review of the computer industry indicated that it has completed four generations and is now entering its fifth generation. Engineers have labeled computers that use the vacuum tubes as the first generation computers, and those that used the transistors and diodes as the second generation of computers. The integrated circuits (ICs) ushered in the third generation computers. Currently we are enjoying the benefits of the fourth generation computers that were made possible thanks to the development of micro-processors.

Arguably, the fifth generation of computers is already with us. The development of integrated 'software and multiprocessors', of the type facilitated by field programmable gate arrays (FPGA) and others, are ushering a new generation of 'Peta-scale' computers. In principle, computer engineers have developed a common consensus on the path toward the fifth generation of computer based systems. This path involves the global unification of software components that interacts with a series of hardware coprocessors. The fifth generation of computers is expected to deliver performances in the order of petabytes (storage capacity in the order of 10 million or more gigabytes) and pataflops (one quadrillion floating point operations per second). In the US, the National Science Foundation and DARPA have initiated funding for the development of such computers. In fact, DARPA has contracted with IBM through the PERCS (Productive, Easy-to-Use, and Reliable Computer System) program. Other countries, such as, China, Germany and Japan, have similar programs. The immediate computational focus of the 'Peta-scale' computers under development will be on weather and climate simulations, nuclear and quantum chemistry simulations, and cosmology and fusion science simulations.

The motivation of the research program described herein is geared towards the development of a Computational Fluid Dynamic tool that seeks to maximize the benefits of future 'Peta-scale' computers.

2 A HISTORIC VEIW OF CFD AS AN INDUSTRIAL DESIGN TOOL

A historic view of the Fluid Dynamic industry, especially, as it relates to the aerospace industry, indicates that there are at least three major breakthroughs in CFD. The first breakthrough occurred in the 1950's and 1960's. During this period, numerical methods and grid generation techniques were merged into the formation of Computational Fluid Dynamics (CFD) as a special branch of fluid mechanics. However, in the 1950s and 1960s CFD did not play a dominant role, mainly due to the lack of computational facilities. Nevertheless, numerical methods were developed and applied to 2D flows. In those days, the results were always supported by experimental data, thus validating the importance of CFD.

A second breakthrough in CFD occurred in the 1970s, when the science of orthogonal surface-fitted structured grids was introduced. During that time, the storage and speed of selected and limited digital computers were sufficient to conduct CFD studies on flow problems of practical interest. Using structured surface-fitted grids, the computations of flow over airfoils and wings became accurate, affordable and efficient. This breakthrough led to remarkable improvements in the design and performance of fixed wing aircrafts.

The third breakthrough in CFD occurred in the 1980s and 1990s. During this time, the computer had fully penetrated the industrial market and was well on its way to making it in every home. In addition, there were remarkable improvements in both computational speed and storage. At this time, numerical algorithms and grid generation techniques were expanded to included unstructured grids on realistic aircraft

configurations. The successful aerodynamic analysis of the full size aircraft configurations using CFD was demonstrated, [2]. It was also in the 1990s that CFD penetrated into other industries, such as, the automobile, civil and environmental industries.

CFD as a design tool is playing a leading role wherever a flow field is being analyzed. CFD has significantly influenced the way engineers analyze problems and conduct design. However, not withstanding these successes, there are still great CFD challenges remaining today [4,5].

3 THE CHALENGES OF THE CFD INDUSTRY

Typically, any problem facing the CFD engineer can be solved through the integrated use of the following three elements [6,7,8,9,10]:

(i) the available or intended computational hardware,
(ii) an appropriate form of the conservation laws and their constitutive relations, and
(iii) a specified set of computational grid points.

As such, to understand the challenges facing the CFD industry, one must put these three elements in proper perspective.

3.1 Conservation Laws and Their Constitutive Relations

The computational hardware of interest to this research was described in the introduction section of this paper. The motivation of the research program described herein is geared towards the development of a Computational Fluid Dynamic tool that seeks to maximize the benefits of future 'Peta-scale' computers.

3.2 Conservation Laws and Their Constitutive Relations

The conservation laws and their constitutive relations are usually specified by the CFD designer. In most instances, these equations are chosen based on the capability of the available computational hardware and in the case of an industrial software, the available trubulence model. The appropriate form of the conservation laws and their constitutive relations of interest to this research is the Navier-Stokes equation with the Reynolds Stress Model. The relevance of turbulence models is becoming a very significant issue in CFD simulations. Designers are currently focusing on problems where turbulence has the dominant effect and problems where the traditional two-equation models are no longer adequate. Clearly no proper evaluation of the merits of different turbulence models can be made unless the discretisation error of the numerical algorithm is known. As such, grid sensitivity studies are crucial for all turbulence model computations, including the RSM.

3.2.1: Reynolds stress transport models

The Reynolds stress transport models (RSM) dispense with the notion of turbulent viscosity, and determine the turbulent stresses directly by solving a transport equation for each stress component. This process requires the solution of six additional equations that are coupled to the Navier-Stokes equations, along with an equation for ε to provide a length scale [11,12,13]. In a similar manner, the turbulent heat fluxes are determined by solving three coupled equations; one for each flux component.

In principle, the RSM can simulate complex strains and non-equilibrium flows. Based on today's standards, RSM is expensive to compute. In addition, RSM is complex, requiring boundary conditions for each of the new parameters, which can lead

to problems of convergence. For these reasons it has not yet been widely adopted as an industrial tool.

3.3 Computational Grid Points

The successful analysis of any CFD design problem can be traced back to the successful development of its grid structure. As such, in order to appreciate the challenges facing the CFD Industry one must take a critical look at the grid generation techniques available. Typically, the grid generation procedure is left up to the CFD designer, who has one of two choices, structured or unstructured grids methods.

3.3.1: Structured Grid Methods

Structured grid methods take their name from the fact that the grid is laid out in blocks of regular repeating pattern. These grids utilize quadrilateral elements in 2D and hexahedral elements in 3D. Although the element topology is fixed, the grid can be shaped to be body fitted through stretching and twisting of the block. In reality, structured grid tools utilize sophisticated elliptic equations to automatically optimize the shape of the mesh for orthogonality and uniformity. Structured grids can be arranged in multiple blocks, with and without overlapping. Refer to Figure 1.

Structured grids enjoy a considerable advantage over its unstructured conterpart, in that they allow a high degree of control. In addition, hexahedral and quadrilateral elements, tolerates a high degree of skewness and stretching without significantly affecting the solution accuracy in the case of well behaved flowfields. In addition, structured block flow solvers typically require the lowest amount of memory for a given mesh size and execute faster because they are optimized for the structured layout of the grid. The major drawback of structured block grids is the time and expertise required to lay out an optimal block structure for industrial size model. Grid generation times are usually measured in days if not weeks.

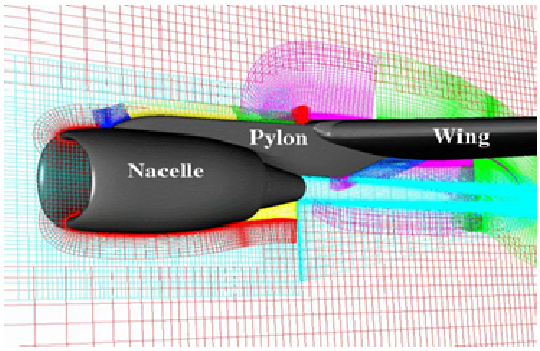

Figure 1: Structured Overlapping Grids [3].

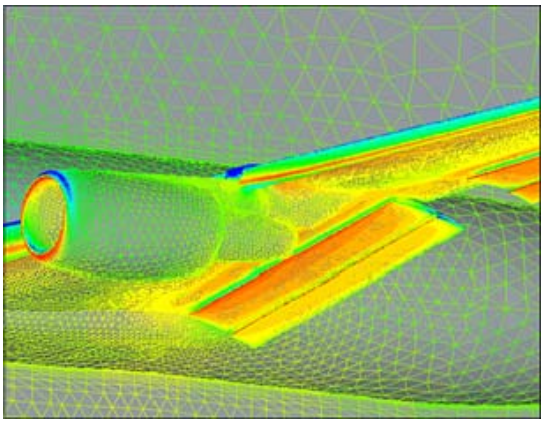

Figure 2: Unstructured Grids [3].

3.3.2: Unstructured Grid Methods

Unstructured grid methods utilize an arbitrary collection of elements to fill the domain. Because the arrangement of elements have no discernible pattern, the mesh is called unstructured. Refer to Figure 2. These types of grids typically utilize triangles in 2D and tetrahedra in 3D. As with structured grids, the elements can be stretched and twisted to fit the domain. These methods have the ability to be automated to a large

degree. Given a good CAD model, a good mesher can automatically place triangles on the surfaces and tetrahedra in the volume with very little input from the user. The automatic meshing algorithm typically involves meshing the boundary and then adding points in the interior. The advantage of unstructured grid methods is that they are easily automated and, therefore, require little user time or effort. The user need not worry about laying out block structure or connections. Unstructured methods also enable the solution of very large and detailed problems in a relatively short period of time. Grid generation times are usually measured in minutes or hours.

The major drawback of unstructured grids is the lack of user control when laying out the mesh. Typically user involvement is limited to the boundaries. In addition, triangle and tetrahedral elements are resistant to stretching and twisting, therefore, the resulting grids are isotropic, with all elements having roughly the same size and shape. This is a major problem when trying to refine the grid in a local area, often the entire grid must be made much finer in order to get the point densities required locally. Another drawback of this method is its reliance on geometric input or CAD data. Typically, most meshing failures are due to some minuscule error in the geometric input. Unstructured flow solvers typically require more memory and have longer execution times than structured grid solvers on a similar mesh.

3.4 Hybrid Cartesian Grid Flow Solver Approach

The pros and cons of the state-of-the-art in grid generation science outlined in section 3.3, and the potential computational capabilities of the next generation computers outlined in section 1 provide a significant opportunity for the CFD industry [14,15]. Opportunities exist to overcome the existing challenges of grid generation and to boldly tackle the direct simulation of turbulent dominated flows over complex configurations.

Reductions in aircraft design cycle times through the automated generation of structured grids with optimum surface resolution can be achieved. These reductions will most likely come not from increased reliance upon user interactive methods, but instead from methods that can be fully automated and incorporated into ‘black box’ packages. In comparison with unstructured grid methods, three-dimensional Cartesian grid approaches are still in its infancy. However, limited experiences with automated Cartesian grid generation techniques are quite promising. Our research is targeted at furthering the development of Cartesian methods so that they can become key elements of a completely automatic and coupled grid generation and flow solution procedure. The package must also be applicable to the aerodynamic analysis of complex aircraft geometries.

Cartesian approaches are of course beset with their own unique difficulties. The most challenging is the removal of the body-fitted grid constraint. This allows the Cartesian hexahedra used to discretize the flow field and to intersect the surface in an arbitrary manner. Successful research into the development of robust procedures for the efficient creation and distribution of the hexahedra will produced an automatic procedure for Cartesian grid generation. Another potential benefit of this research is the ability to solve complex turbulent flow fields with RSM over industrial size configurations afforded by the simplicity of Cartesian grids.

4 CURRENT RESEARCH FOCUS

The immediate phase of this research is focused on the development of a robust, efficient, and accurate numerical framework that is capable of solving a variety of

complex fluid dynamics problems [16,17]. The new scheme is built with extensive physics considerations and has the following features:

i. The numerical scheme is based on the solution of the integral form of the Navier-Stokes equation. This approach focuses on the benefits of the traditional finite volume and finite difference schemes, and therefore guarantees the conservation properties throughout the domain by the first and the formulation simplicity by the latter.

ii. The Cartesian grid generation procedure is used to develop spacial and temporal control volumes upon which the integral form of the physical conservation laws are applied. As such, the scheme has the potential to satisfy the physical realities of fluid fluxes for both time and space.

iii. Accounting of the mass, momentums, and energy fluxes (both within the control volume and through its surfaces) is conducted with the aid of the mean value theorem, rather than the traditional extrapolation or interpolation of the node's information from neighboring cells.

iv. The accuracy and efficiency of the scheme is demonstrated on flows with rectangular boundries.

4.1 The Governing Equations

The equations that govern fluid flows and the associated heat transfer are the continuity, momentum and energy equations. These equations were independently constructed by Navier (1827) and Stokes (1845), and are referred to as the Navier-Stokes equations. In this research, the integral forms of the Navier-Stokes equations, (1–3) are of paramount importance. The continuity, momentum and energy equations are listed as follows:

$$\iiint_v \frac{\partial \rho}{\partial t} dv + \iint_s \rho \bar{V} d\bar{s} = 0 \tag{1}$$

$$\frac{\partial}{\partial t} \iiint_v \rho \bar{V} dv + \iint_s \left(\rho \bar{V} . d\bar{s}\right) \bar{V} = - \iint_s P d\bar{s} + \iint_s \hat{\tau} d\bar{s} \tag{2}$$

$$\frac{\partial}{\partial t} \iiint_v \rho E dv + \iint_s \rho E \bar{V} . d\bar{s} = - \iint_s P \bar{V} . d\bar{s} + \iint_s \hat{\tau} . \bar{V} d\bar{s} + \iint_s \bar{\dot{q}} d\bar{s} \tag{3}$$

In Equations (1) the symbols, ρ, v, t, represent the density, the volume of a control fluid element, and time, respectively. In addition, the symbols, $\bar{V}$, $d\bar{s}$ and $\dot{q}$, in equations (1) (2) and (3) represent the fluid velocity, the surface of the control volume and the local heat transfer rate. In this research, fluid velocity and the surface element are described through the use of vector quantities as follows:

$$\bar{V} = u\bar{i} + v\bar{j} + w\bar{k} \tag{4}$$

$$d\bar{s} = dydz\bar{i} + dxdz\bar{j} + dxdy\bar{k} \tag{5}$$

$$\bar{\dot{q}} = \dot{q}_x \bar{i} + \dot{q}_y \bar{j} + \dot{q}_z \bar{k} \tag{6}$$

In equations (2) and (3), the symbol, P, represents the pressure and the symbol, $\hat{\tau}$, represents a symmetric tensor that defines the various components of the local viscous stresses. This symmetric tensor is described by the equation:

$$\hat{\tau} = \begin{bmatrix} \tau_{xx} & \tau_{xy} & \tau_{xz} \\ \tau_{yx} & \tau_{yy} & \tau_{yz} \\ \tau_{zx} & \tau_{zy} & \tau_{zz} \end{bmatrix} \tag{7}$$

where the symbols of the six independent components, $\tau_{xx}, \tau_{xy}, \tau_{yy}, \tau_{yx}, \tau_{zx}, \tau_{zy}$ and τ_{zz}, are the local shear stress that were defined in [4,5] as follows:

$$\tau_{xx} = \frac{2}{3}\mu(\nabla.V) + 2\mu\frac{\partial u}{\partial x} \tag{8}$$

$$\tau_{yy} = \frac{2}{3}\mu(\nabla.V) + 2\mu\frac{\partial v}{\partial y} \tag{9}$$

$$\tau_{zz} = \frac{2}{3}\mu(\nabla.V) + 2\mu\frac{\partial w}{\partial z} \tag{10}$$

$$\tau_{xy} = \tau_{yx} = \mu\left(\frac{\partial u}{\partial y} + \frac{\partial v}{\partial x}\right) \tag{11}$$

$$\tau_{xz} = \tau_{zx} = \mu\left(\frac{\partial u}{\partial z} + \frac{\partial w}{\partial x}\right) \tag{12}$$

$$\tau_{yz} = \tau_{zy} = \mu\left(\frac{\partial w}{\partial y} + \frac{\partial v}{\partial z}\right) \tag{13}$$

The symbols, $\dot{q}_x, \dot{q}_y$ and $\dot{q}_z$, in equation (6) represent the components of the heat flux vector in the *x*- , *y*-, and *z*-directions, respectively. These components are defined by Fourier's law, and expressed mathematically as,

$$\begin{aligned} \dot{q}_x &= -k\frac{\partial T}{\partial x} \\ \dot{q}_y &= -k\frac{\partial T}{\partial y} \\ \dot{q}_z &= -k\frac{\partial T}{\partial z} \end{aligned} \tag{14}$$

The symbols, *P* and *E*, in equations (2) and (3) are defined as follows:

$$\begin{aligned} P &= \rho RT \\ E &= C_v T + \frac{u^2 + v^2 + w^2}{2} \end{aligned} \tag{15}$$

where R is the gas constant. The symbols, μ and *k*, represents the viscous and thermal properties of the fluid of interest. In this analysis, the viscosity of the fluid is evaluated through the use of Sutherland's law, [4,5],

$$\mu = \mu_\infty \left(\frac{T}{T_\infty}\right)^{3/2} \frac{T_\infty + 110}{T + 110} \tag{16}$$

μ_∞ and T_∞ are freestream values.

In the case of 3D aerodynamic analysis, the Navier-Stokes equations (1)–(3) defined above can be treated as a closed system of five equations relative to five unknowns. The unknows are the folowing five primitive flow field variables: $[\rho,\ u,\ v,\ w,\ T]$. The immediate goal of this research is to developed an explicit method that solves the Navier-Stokes system of equation as defined herein.

5 THE METHOD OF CONSISTENT AVERAGES

In the developmental stages of this research, a typical fluid flow is represented by a rectangular domain [1]. This spatial computational domain is further divided into a collection of elementry cells or 'spatial' cells. These cells are chosen as infinitesimal rectangular prisms, with unit normal, **ñ**, in the *x*, *y*, and *z* directions. The dimensions of each side of a cell are defined by *dx*, *dy*, and *dz*, respectively. Refer to Figure 3. Further, a given cell is defined locally by six independent surfaces, and each surface defined by four points or nodes in a given plane. Additionally, plus and minus notations are use to define the unit normal, **ñ**, with respects to each surface. Next, each surface of each cell is defined by four nodes; namely, nodes-1, nodes-2, nodes-3 and nodes-4. Figure 3 illustrates the plus and minus notations for the surfaces with normal to the *z*-direction. It is of interest to note that the use of the object oriented programming concept makes it very convenient to use identical surface objects in the *x* and *y* directions.

In anlogous to 'spatial' cells, the concept of 'temporal' cells are also introduced. The 'temporal' cells are defined as rectangular prisims formed from the center points of eight neighbouring 'spatial' cells. Finaly, a fluid control volume is defined, as a collection of eight 'spatial' cells and one temporal cell. A typical control volume is illustrated in Figure 4.

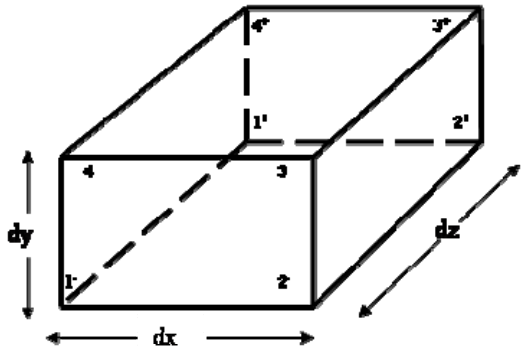

Figure 3: Spatial Cell with Notation at Surface Nodes.

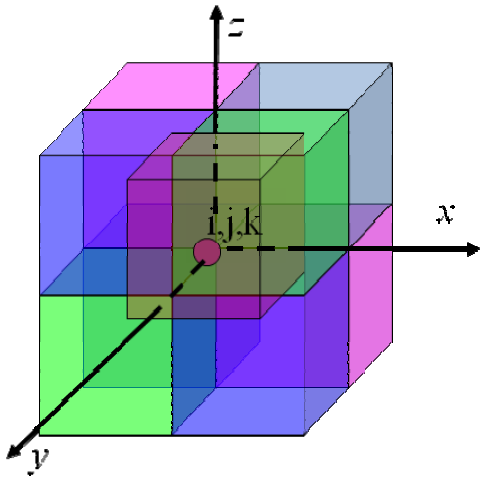

Figure 4: Illustration of Control Volume.

Each term in the Navier-Stokes equations (1)–(3) are applied systematically to each spatial cell. The mean value theorem is invoked and a set of algebraic equations representing the rate of change of mass, momentum, and energy associated with each spatial cell is derived. However, the rates of change of the time-fluxes are not associated with any grid point, but with the 'spatial' cell. When the spatial cells are pieced together to form a temporal cell within the control volume, the arithmetic average of the rates of change within the temporal cell then defines rates of change at the *ijk*-point of interest.

It is of interest to note that the plus and minus surfaces in each direction are adequate to evaluate the invicid fluxes. However, two additional and adjacent surfaces in each directions are needed for evaluating the viscous terms. Nevertheless, in the

analysis, these surfaces are denoted as the plus-plus and minus-minus surfaces, and are treaded in the manner described earlier.

5.1 Application of the Conservation of Mass to a Spatial Cell

To demonstrate the utility of this numerical approach to fluid dynamic problems, consider a typical flow through the surfaces of an infinitesimal spatial cell, as illustrated in Figure 5. In general, the fluid flows arbitrary in all directions. Even though the *Method of Consistent Averages* (*also refered to as the Integral-Differential Scheme 'IDS [1]'*) has the potential to solve 2D or 3D fluid-flow problems, for the purpose of illustration, the discussions conducted in this paper are limited to a 2D fluid flow application.

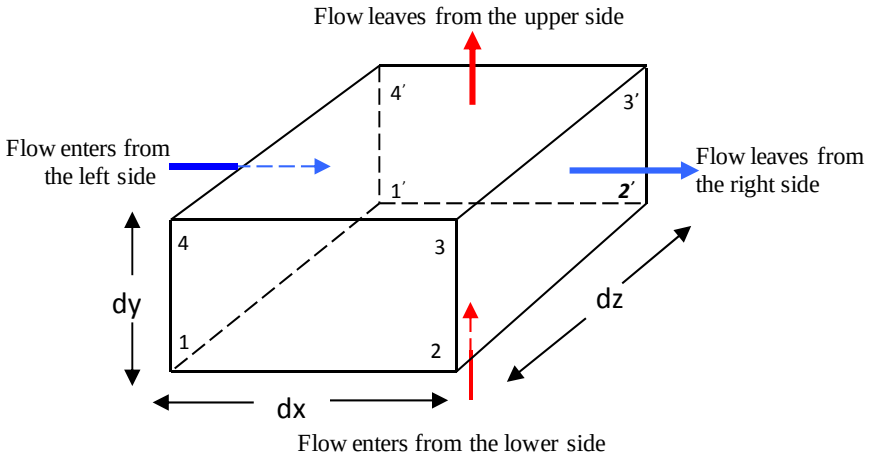

Figure 5. A Typical Flow through the Surfaces of Control Volume

When describing the 2D approach of the *Method of Consistent Averages*, a major challenge involves the conversion of the naturally 3D conservation laws into their 2D counterparts that maintain the integrity of the 3D flowfield and its associated effects. To achieve this goal, two scientific assumptions were made. They are as follows:

i. Using the Cartesian system of coordinates, the spatial cells are chosen as infinitesimal rectangular prisms, with unit normal, **ñ**, in the *x*, *y*, and *z* directions.
ii. It is assumed that no flow occurred in the z-direction. In addition, the dimension, dz, of a typical control volume is always a single unit, ie., dz = 1.

These assumptions led to the fact that the fluid properties in the z-direction across any cell are constants and the net flow of mass, momentum, and energy in the z-direction is always zero. Consequently, in all surface integration processes, all pertinent terms that are associated with the z-directions as required by the conservation laws are neglected.

Armed with these two assumptions, the governing equations were converted into their non-dimensional form and applied on each small control volume. The algebraic forms of the rate of change of mass, momentum, and energy at the center of each control volume are formulated as follow:

$$\left(\frac{\partial \rho}{\partial t}\right)_{Center\ of\ cell}^{average} = \left[\begin{array}{l} \dfrac{\left((\rho u)_1+(\rho u)_4\right)-\left((\rho u)_2+(\rho u)_3\right)}{2\Delta x} \\ + \\ \dfrac{\left((\rho v)_1+(\rho v)_2\right)-\left((\rho v)_3+(\rho v)_4\right)}{2\Delta y} \end{array}\right] \quad (17)$$

5.2 Explicit Time Marching Process

The explicit time matching process associated with the *Method of Consistent Averages* is conducted based on the taylor series expansion formulation as follows [1]:

$$U_{i,j,k}^{t+\Delta t} = U_{i,j,k}^{avg,t} + \left(\frac{dU}{dt}\right)_{i,j,k}^{avg,t} \Delta t \quad (18)$$

where the time flux vector, U, is defined at each *ijk*-point, such that, $U = \left[\rho \quad \rho u \quad \rho v \quad \rho v \quad \rho E\right]^T$. The terms on the right of equation (18) are not defined at an *ijk*-point but rather from the control volume and the temporal cell associated with each ijk-point. The term, $U_{i,j,k}^{avg,t}$, is the average value of the flux quantities associated with the control volume surrounting the *ijk*-point. Refer to Figure 5. Where as, the time derivative term, $\left(\frac{dU}{dt}\right)_{i,j,k}^{avg,t}$, is associated with the average rate of change of temporal fluxes associated with the temporal cell at the *ijk*-point.

Since the *Method of Consistent Averages* is an explicit numerical technique for the Navier-Stokes equations, the time step, Δt, is subjected to a stability criterion. This criterion is determine by the following form of the Courant-Friedrichs-Lewy (CFL) relationship,

$$\Delta t_{i,j,k} = C\left[\frac{\left|u_{i,j,k}\right|}{\Delta x}+\frac{\left|v_{i,j,k}\right|}{\Delta y}+a_{i,j,k}\sqrt{\frac{1}{\Delta x^2}+\frac{1}{\Delta y^2}}+\frac{2}{\mathrm{Re}_L}\nu'_{i,j,k}\left(\frac{1}{\Delta x^2}+\frac{1}{\Delta y^2}\right)\right]^{-1} \quad (19)$$

The constant, C, in equation (19) is defined in the range of $0.5 \le C \le 0.8$, and the symbols, $a_{i,j,k}$ and $\nu'_{i,j,k}$, represent the local speed of sound and dynamic viscosity. In this analysis, $\nu'_{i,j,k}$, is evaluated as follows [4,5]:

$$\nu'_{i,j,k} = \max\left[\frac{\frac{4}{3}\mu_{i,j,k}, \left(\gamma\mu_{i,j,k}/\mathrm{Pr}\right)}{\rho_{i,j,k}}\right] \quad (20)$$

6 PRELIMINARY RESULTS

As described earlier in this paper, the immediate goal of this research effort is to develop a computational tool that accurately solves the Navier-Stokes equations in the Cartesian system of coordinates. In this section, the following three standard CFD problems in 3D are solved to demonstrate the validity of the new computational tool:

i. Hypersonic Boundary Layer Interaction Problem
ii. Incompressible Lid Driven Cavity flow Problem
iii. Shock Train Problem

The solution procedure adopted during the numerical simulation of these problems is as follows:

i. The physical domain of the problem is defined in Cartesian Coordinates.
ii. The freestream parameters of interest (M, Re, Pr, etc.) are mapped to fit the Navier-Stokes equations requirements and the physical domain described in 1.
iii. The boundary conditions are assigned in accordance with *Method of Consistent Averages* methodology.
iv. The solution grid and initial solution are auto-generated.
v. The solution data is extracted from the 3D domain through planes and lines at the locations of interest.

7 HYPERSONIC FLOW OVER A FLAT PLATE

This section focuses on a developing boundary layer on a flat-plate under supersonic conditions. An oblique shock wave develops at the leading edge of the flat plate due to the viscous boundary layer effects. Refer to Figure 6. The occurrence of the boundary layer often provokes dramatic changes in the flow field features, both qualitatively and quantitatively. Important consequences of this occurrence are the increase in the skin friction coefficient and the shear stresses inside the boundary layer region. Moreover, dissipation of kinetic energy within the boundary layer can cause high flow-field temperatures and thus high heat-transfer rates. The supersonic flow over a flat plate is a classical fluid dynamic problem, and it has received considerable attention from many researchers; including Anderson [4,5], Akwaboa [17], MacCormack [18] and Rasmussen [19].

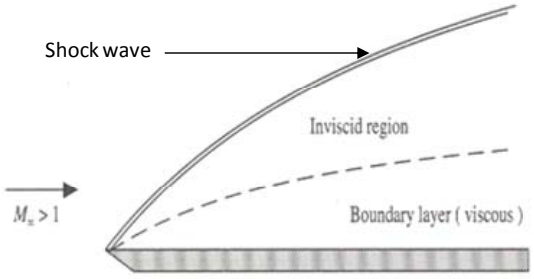

Figure 6: Hypersonic Boundary Layer [4]

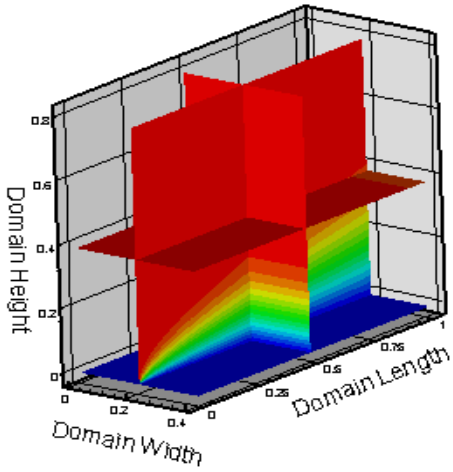

Figure 7: 3D Hypersonic Flowfield [1]

7.1: Freestream and Convergence Conditions

A 3D flow at Mach number 4.0 is considered. The specific heat ratio, γ, is set to 1.4, and the Prandtl number, Pr to 0.71. The freestream density, temperature, viscosity, and speed of sound are set to 1.25518 kg/m^3, 288.18 k, 1.7894*10.0E-5 kg/m.s, and 340.28 m/s, respectively. The Reynolds number is 9.3191*10.0E+7, based on a 1.0 m high flow field The flow field domain is 1.2m by 1.0 m.

The non-dimensional algebraic form of the mass, momentum, and energy equations derived in section 4 and outlined in section 5, are used to develop the numerical solution. It should be noted that when evaluating the viscous terms $\tau_{xx}, \tau_{yy}, \tau_{zz}, \tau_{xy}, \tau_{xz}, \tau_{yz}, \dot{q}_x, \dot{q}_y, and\ \dot{q}_z$ at the inflow, and symmetry boundaries, the forward differencing approximation was used. The backward differencing approximation was used to evaluate these quantities at the far-field and outflow boundaries. For all internal points, these terms are evaluated according to the procedure described earlier. The solution marches in time from the initial conditions until it converged to the steady state condition. The convergence was considered to occur when the maximum residual of the mass, momentum, and the energy fluxes at each internal grid point changed no more than $10E^{-15}$ between time steps. Mathematically, the maximum residual of the fluxes is calculated as the difference between the new and the old value of the flux for each two consecutive time steps, such that,

$$residual = \max \begin{bmatrix} (Mass\ residual)_{i,j,k}, \\ (X\_momentum\ residual)_{i,j,k}, \\ (Y\_momentum\ residual)_{i,j,k}, \\ (Z\_momentum\ residual)_{i,j,k}, \\ (Energy\ residual)_{i,j,k} \end{bmatrix} \tag{20}$$

7.2 Flat Plate Laminar Flow Results

Figure 8 illustrates the 3D distribution of the *x* component of the velocity on three perpendicular XY, XZ, and YZ planes. The planes intersect at the mid point of the domain. Another XZ plane at y = 0 is plotted to show the solid boundary on the plate surface. As expected the velocity distribution starts from the zero on the plate surface due to the no slip boundary condition and increase gradually until it reaches the freestream value out side the boundary layer zone. The boundary layer is along the XY plane parallel to the flow direction. The velocity reaches its freestream value before the mid point along the domain height.

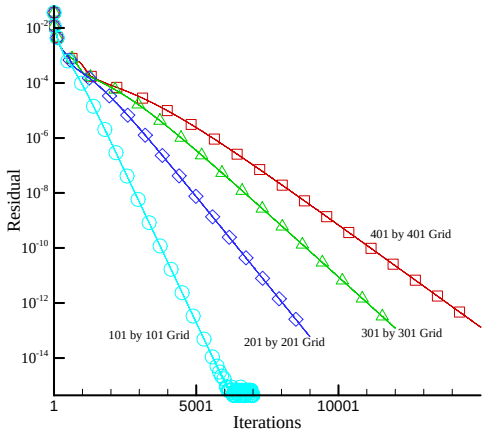

Figure 8: Residual Error vs. Time

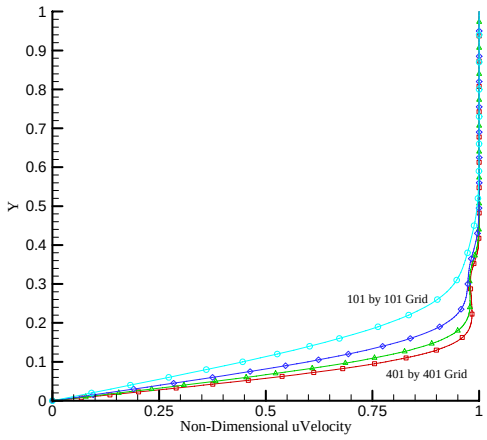

Figure 9: The exit u-Velocity component

7.3 Code Validation Studies

It is of interest to note that even though the flat plate problem was solved in a 3D domain, the boundary conditions on the side surfaces were set so as to produce a 2D solution. This was done mainly for code validation purposes. First and foremost, grid validation studies were conducted. This study was conducted over a series of grids, rangening from 101 by 101 nodes to 501 by 501 nodes. During these studies, the behavior of the independent flow field variables, r, u, v and T, were observed. The results of this study are illustrated in Figures 8 through 11, where the behavior of the flow field variables, r, u, v and T, were documented.

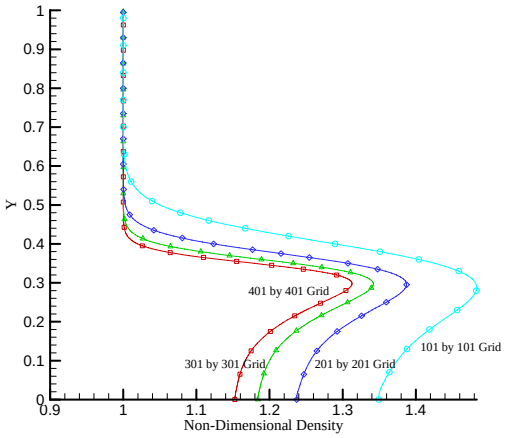

Figure 10: The exit Temperature in Boundary Layer

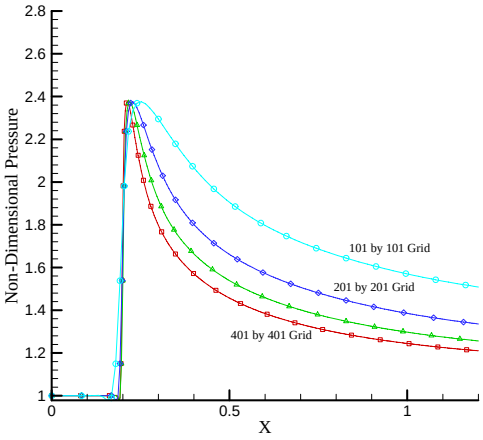

Figure 11: Pressure distribution in Boundary Layer

The residual as a function of the number iterations are plotted in Figure 8, for each grid size described earlier. In each case, ther results were consistent, the residual error, refer to equation (20), exponentially decreased with respects to time. Also common in these illustrates, the flow field variables all approached a steady solution as the grids get finer.

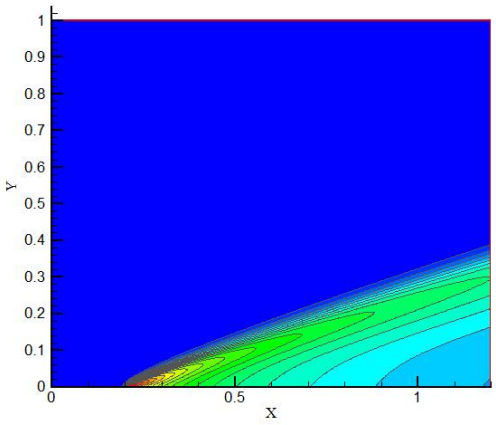

Figure 12: Density distribution in Boundary Layer

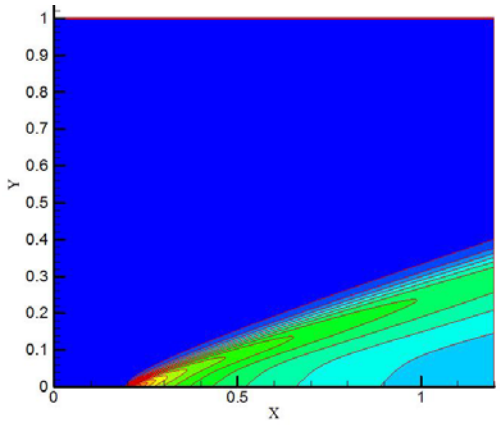

Figure 13: Pressure distribution in Boundary Layer

Of importance also to note, is the fact that the pressure distributions shows that the magnitude of the shock wave was capture in the coarse grid. However, the coarse grids over predictes the flow field variables, r, u, v and T, in all cases, including the

boundary layer height. Finally, contour plots of the flow field variables were developed using data from the fine grids, 401 by 401, and illustrated in Figures 12 – 15. The results illistrated in Figures 12 – 15, illustrates that the boundary layer and the shock wave emminates from the the leading edge of the plate. Moreover, there is no clear boundary layer, but a 'shock layer', where the shock wave and the boundary layer are totally merged.

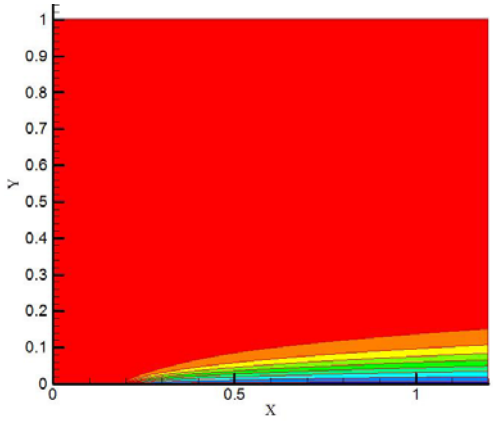

Figure 14: u-Velocity distribution in Boundary Layer

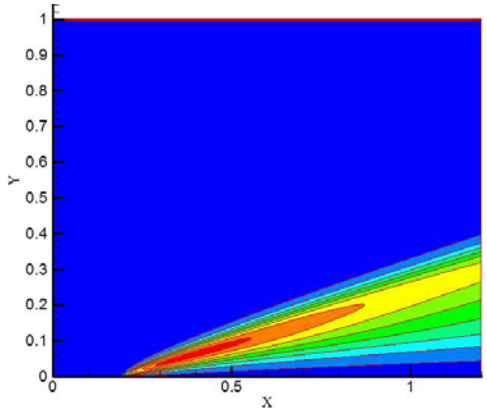

Figure 15: v-Velocity distribution in Boundary Layer

8 THE LID DRIVEN CAVITY PROBLEM

Consider a 3D incompressible flow field that is confined to a cavity, where the motion in the cavity is generated by the sliding motion of the fluid at a plane of one of its surfaces. This moving fluid surface generates vorticity which diffuses inside the cavity. The diffusion effect now becomes the dominant mechanism driving the flow. As part of the validation studies of the Navier-Stokes code developed herein, the lid driven cavity problem was solved. Figures 16 and Figure 17 presents results obtained from the IDS method and compares this results to that found in Choi & Merkle [20] and Vigneron et.al [21].

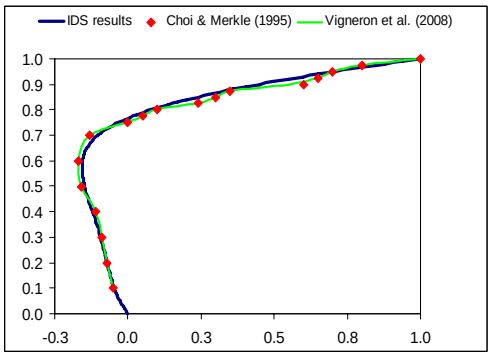

Figure 16. The *x* Component Velocity Profile along the Vertical Centerline of the Cavity

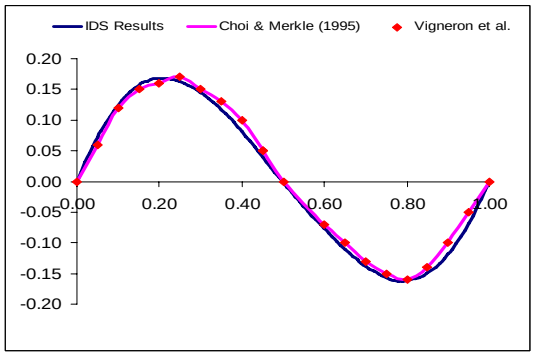

Figure 17. The *y* Component Velocity Profile along the Horizontal Centerline of the Cavity

The data presented are the steady state solution for the *x-component* of the velocity on the vertical centerline and the *y-component* of the velocity on the horizontal centerline of the cavity. It is of interest to note that incompressible solutions are

obtained without introducing any modifications to the algorithm. Figures 18 and 19 present streamlines comparison between the IDS solution and Vigneron et.al [21]. solution for the cavity problem under the same operating conditions. The IDS solution shows very good agreement with the results of Choi & Merkle [20], and Vigneron et al [21].

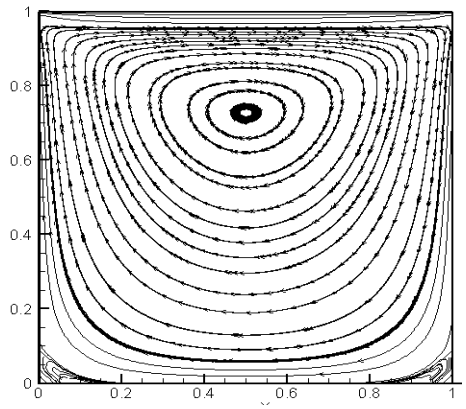

Figure 18. Cavity Streamlines plot of the IDS Solution

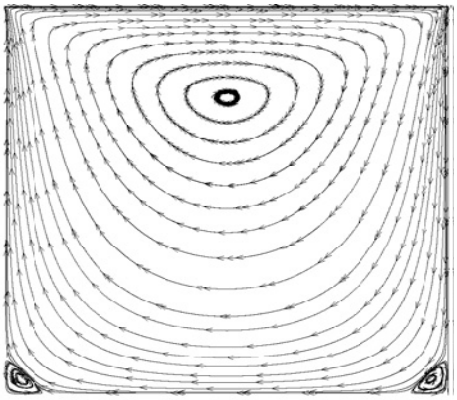

Figure 19. Cavity Streamlines plot Vigneron Solution

To study the effect of the boundary conditions on the solution, the *x component* velocity distribution on the mid XY and YZ planes in the domain is plotted in Figure 20. As in the figure for the wide container case, the flow seems to be symmetric around the mid XY plane and there no any effect of the boundary parallel to the direction of the flow. When a finite width of the container is considered and the solid boundary is enforced on the planes parallel to the direction of the flow, the influence of the boundary force the particles to twist while it is moving and the three dimensional flow is simulate more accurately in this case.

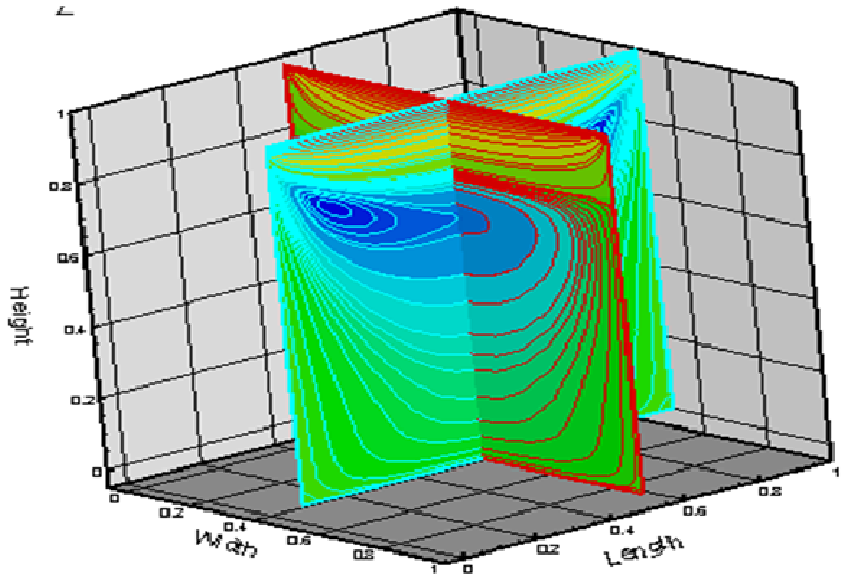

Figure 20. The *x* Component Velocity Distribution on the Mid XY and YZ planes [1].

9 DEFINITIONS OF SHOCK TRAIN AND PSEUDO SHOCK

A characteristic of supersonic internal flows is the development of a strong shock wave that forms as a result of the flow interaction with the boundary layer along the wall surface of the device. The shock is bifurcated and a series of repeated shocks is formed along the flow passage. The number of these shock series and their position in the flow passage is dependent on the freestream Mach number, the pressure conditions imposed at both the upstream and downstream locations of the flow passage, the passage geometry, and the wall friction due to viscosity. This phenomena was described in Om et al [22] as '*multiple shocks*', by McCormick [18], as a '*shock system*', and most recently by Carroll and Dutton [23], and Matsuo [24] as a '*shock train*'. Through the interaction region, the flow can be decelerated from a supersonic flow to a subsonic flow. Figure 21 presents an illustration of the shock train phenomenon in an internal duct. The shock train is clearly visible and is usually followed by an adverse pressure gradient region in a long enough duct. The interaction region including both shock train and the subsequent pressure recovery region is referred to as a '*pseudo shock*'.

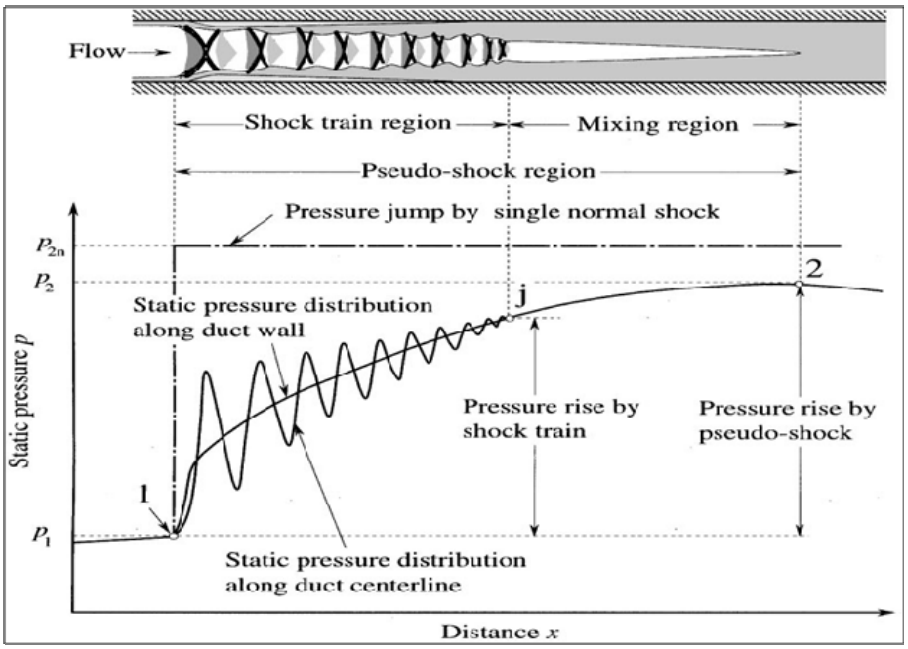

Figure 21. Schematic of Shock Train and Pseudo Shock [23]

Also presented in Figure 21 is the behavior of the static pressure at the wall and at the center line of the constant area duct. Examination of this figure revels that the static wall pressure rises at a faster rate in the shock train region, i.e. between points 1, *j*, than in the mixing region, i.e. between points *j*, 2. A similar trend (pressure rise) is observed in the static pressure distribution along the duct centerline. The oscillations observed in the static pressure distribution along the duct centerline are due to the presence of the successive shock series or shock train. Beyond point j no shock exists and the pressures at the wall surface and at the centerline are essentially the same.

The pressure rise between the points 1 and *j* is caused by the shock train. If the flow is fully subsonic and uniform at the point *j*, then the static pressure downstream of this point should decrease due to the frictional effect. However, it should be noted that

the shock train is followed by the "mixing region", where no shocks exist. The pressure increase in this region is due in some extent to the mixing of a highly non-uniform profile created by the shock train. The static pressure reaches its maximum at point 2.

9.2.1 IDS Solution results to the Shock Train Problem

The pressure behavior along the duct centerline and along the duct wall for shock train was described in the preceding section. IDS solution results to the shock train problem is now presented in Figures 22 and 23. Validation of the IDS solution to the shock train problem is accomplished with the use of the experimental and numerical results obtained by Carroll et al. In their numerical computation they used the Baldwin-Lomax algebraic turbulence model and the Wilcox-Rubesin two equations turbulence model [23]. Figure 22 closely reproduces the static pressure behavior results and physics of the shock train problem as presented in Figure 21. Examination of Figure 23 clearly demonstrates that the results obtained from the IDS solution to the shock train problem closely recovers results obtained experimentally and numerically by other researchers in the field.

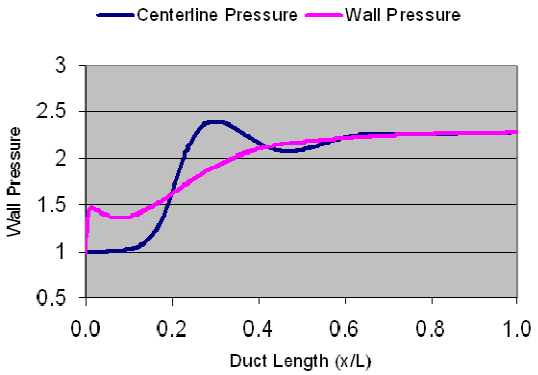

Figure 22: Wall and Centerline Pressure along the Duct Length [1]

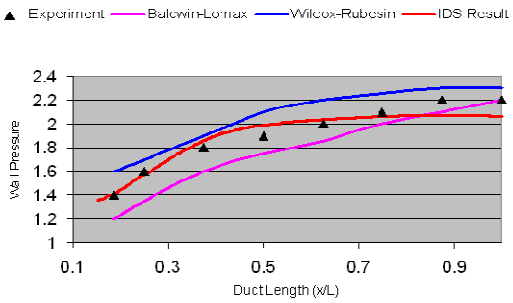

Figure 23: Wall Pressure along the Duct Length

Having validated the IDS methodology, results are now presented in Figure 24 for the Mach number distribution along the mid XY plane. Examination of Figure 24 clearly indicates the presence of the shock train region. The contour lines in this figure shows that the flow changes from a supersonic flow to a subsonic flow across the shock as is expected from the physics of the flow.

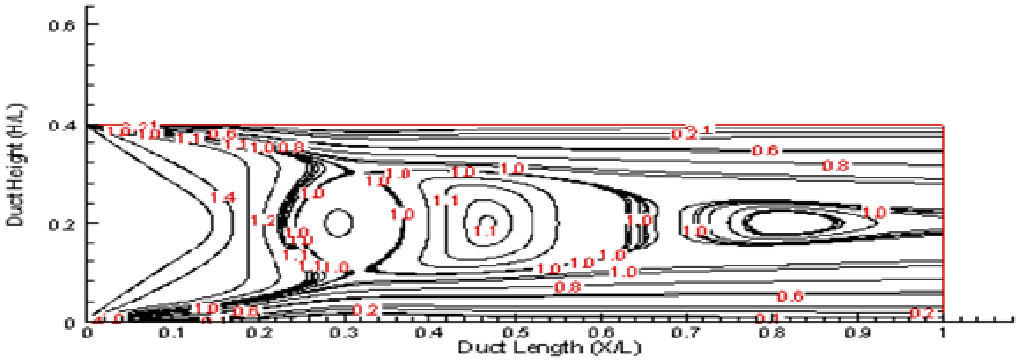

Figure 24: Mach Number Distribution on the Mid XY Plane [1]

10 CONCLUSION

A numerical procedure for solving the 3D Navier-Stokes equations was developed and validated. This procedure is called the Method of Consistent Averages (MCA). In this procedure, the concept of a special control volume was considered as the integral form of the Navier-Stokes equations were implemented to solving fluid flow problems. The numerical procedure was designed to overcome several limitations of traditional finite volume schemes. In addition, the procedure is built on a strong mathematical foundation with extensive physics considerations. The main features of this numerical framework are as follows:

i. The computational domain is descretized in a collection of spatial cells, with eight neighboring cells forming a temporal cell, and a control volume.
ii. The rates of change of the fluxes at the center of each spatial and temporal cell are evaluated based on the conditions immediately outside of its surfaces.
iii. The mean value theorem is used in these all numerical calculations.
iv. As in traditional marching schemes, the evolution of the explicit solution process is based on Taylor's series expansion. Once again, each term in the expansion equation is evaluated based on the mean value theorem.

At this stage of its development, the MCA/IDS numerical procedure was validated through the use of three established flow field problems. These problems are listed as follows: the hypersonic boundary layer problem, the lid driven cavity problem and the pseudo-shock train problem. The solutions generated for these problems using the MCA procedure showed very good agreement with the physical expectations and experimental data for each problem. A CFD literature survey indicated that a large percentage of the compressible flow field solvers encountered convergence difficulties when utilized to solve incompressible flow problems [1]. In an effort to demonstartes it unique capability, the MCA/IDS was used to solve the incompressible lid driven cavity problem. The MCA delivered excellent results for this problem without any convergence difficulties. In addition, the MCA procedure was employed to solve a pseudo-shock train problem. This problem is considered as one of the most challenging problems encountered in computational fluid dynamics [1]. Once again, the MCA procedure predicted excellent results. In conclusion, the solutions obtained for compressible external and internal flows, and the incompressible lid driven cavity problem justify the belief that the MCA procedure is robust, efficient, and capable of solving a variety of complex fluid dynamics problems.

11 ACKNOWLEDGMENTS

This work was partially sponsored by the following agencies; ARO, NIA, AFRL at WPAB, NASA Space Grant, and NASA Glenn. In addition, special appreciation is extended to Dr. Datta Gaitonde and Mr. Donnie Saunders of the Air Vehicles Directorate at Wright Patterson Air Force Base for their encouragement and support of this project. Appreciation is expressed to Dr. Isaiah Blankson of NASA Glenn Research Center and Dr. Reginal Williams of the Naval Airforce Base at Patuxent River in Maryland.

10 REFERENCES

[1] Elamin, Gafar, '*The Integral Differential Scheme (IDS): A New CFD Solver for the System of Navier-Stokes Equations with Applications*', Dissertation 2008.

[2] Bush, Richard J, et al, '*Application of CFD to Aircraft Design*', AIAA paper 86-2651, 1986.

[3] www.spscicomp.org/ScicomP14/talks/Sugavanam.pdf

[4] John D. Anderson, Jr., "*Computational Fluid Dynamics-The Basics with Applications"*, McGraw-Hill, Inc., 1995.

[5] D. A., Anderson, J. C., Tannehill, and R. H., Pletcher, "*Computational Fluid Dynamics and Heat Transfer*", McGraw-Hill Book Co., 1984.

[6] David C., Wilcox, "*Basic Fluid Mechanics*", First Edition, DCW Industries Inc, 1997.

[7] David Pnueli., and Chaim Gutfinger, "*Fluid Mechanics*", Cambridge University Press, 1992.

[8] P. D., Lax, K., and B., Wendroff, "*Systems of Conservation Laws*", Communications on Pure and Applied Mathematics, Vol. 13, PP. 217-237.

[9] R. D., Richtmyer, "*A Survey of Difference Methods for Nonsteady Fluid Dynamics*", NCAR Technical Note 63-2, Boulder, Colorado.

[10] R. W., MacCormack, "*Current Status of Numerical Solutions of the Navier-Stokes Equations*", AIAA paper no. 85-0032, 1985.

[11] D.B. Spalding, "*A Novel Finite Difference Formulation for Differential Expression Involving both First and Second Derivatives*", International Journal of Numerical Methods, Vol. 4, PP. 551–559.

[12] M. Hafez and K. Oshima, "*Computational Fluid Dynamics Review 1998*", Vol. I, II, World Scientific, 1998.

[13] M. Hafez, and D.A., Caughey, "*Frontiers of Computational Fluid Dynamics*", World Scientific, 2005.

[14] U. Ghia, K. N. Ghia, and C. T. Shin, "*High –Resolutions for Incompressible Flow using the Navier-Stokes Equations and a Multigrid Methdod"*, Journal of Computational Physics, Vol. 48, 1982, PP 387-441.

[15] Jiten C. Kalita, Anoop K. Dass, and Nimisha Nidhi, "*An Efficient Transient Navier-Stokes Solver on Compact Nonuniform Space Grids"*, Journal of Computational and Applied mathematics, Vol. 214, 2008, PP 148-162

[16] Gafar Elamin, "*A CFD Scheme Based on a New and Innovative Method of Consistence Averages*", M. S. Thesis, (Department of Mechanical Engineering, North Carolina A & T State University, Greensboro, 2004).

[17] Stephen Akwaboa, "*Navier-Stokes Solver for a Supersonic Flow over a Rearward-Facing Step*", M. S. Thesis, (Department of Mechanical Engineering, North Carolina A & T State University, Greensboro, 2004).

[18] D. C., McCormick, "*Shock/Boundary Layer Interaction Control with Vortex Generator and Passive Cavity",* AIAA Journal, Vol. 31, Issue 1, 1993, PP 91-96.

[19] Maurice Rasmussen, and David Ross Boyd, "*Hypersonic Flow*", John Wiley & Sons Inc., 1994.

[20] Y. H. Choi, C. L. Merkle, "*The Application of Preconditioning in Viscous Flows",* Journal of Computational Physics, Vol. 105, 1993, PP 207-223.

[21] D. Vigneron, J. M. Vaassen, and J.A. Essers, "*An Implicit Finite Volume Method for the Solution of 3D Low Mach Number Viscous Flows using a Local Preconditioning Technique",* Journal of Computational and Applied mathematics, Vol. 215, 2008, PP 610-617

[22] D. Om, and M. E. Childs, "*Multiple Transonic Shock Wave/Boundary Layer Interaction in a circular Duct",* AIAA Journal, Vol. 23, Issue 5, 1985, PP 1506-1511.

[23] B. F., Carroll, and J. C., Dutton, "*Characteristics* of *Multiple Shock Wave/ Turbulent Boundary Layer Interactions in Rectangular Ducts",* Journal of Propulsion and Power, Vol. 6, Issue 2, 1990, PP 186-193.

[24] K., Matsuo, Y., Miyazato, and H. D., Kim, "*Shock Train and Pseudo Shock Phenomena in Internal Gas Flow",* Progress in Aerospace, Vol. 35, Issue 1, 1999, PP 33-100.